NOVEL KINETIC ENERGY PENETRATORS FOR ELECTROMAGNETIC GUNS

Jared L. Hodge*, David L. Littlefield, Stephan Bless, Andrew Short, and Brad Pedersen
The Institute for Advanced Technology
Austin, TX 78759

ABSTRACT

Hypervelocity extending projectiles launched by electric guns are candidates for providing improved lethality to the Future Combat System (FCS). A systematic investigation of rod/tube type extending projectiles shows that optimal performance is achieved with roughly equal partitioning of mass between the two components and with a rod-first orientation. Potential reduction in muzzle energy for defeat of a fixed target is very substantial.

1. INTRODUCTION

The development of advanced heavy vehicle armor poses a severe challenge to direct-fire munitions. The difficulty is compounded for FCS, where mass and recoil constraints limit the bore and muzzle energy of the main gun. Fortunately, within the timeframe of FCS deployment, electromagnetic (EM) guns will become available that can provide increased lethality with reduced recoil.

EM guns operate at hypervelocity without a powder charge, thereby circumventing the recoil and vulnerability problems. Unfortunately, the power supply systems for EM guns can be quite large if the launch energy climbs too high. Novel Kinetic Energy Penetrators (NKEPs) that are engineered to take advantage of the higher launch velocity mitigate this problem by reducing the required launch mass and thus launch energy.

Penetration depth of monolithic cylindrical rods with fixed impact velocity V_i is primarily a function of length L only, increasing as L increases. As such, for rods with constant mass M, if L is increased the diameter D must decrease. When the aspect ratio L/D becomes too large, however, it becomes difficult to launch the projectile from any type of gun system. Large launch L/D can result in large angle of attack α, flexure of the rod, and even failure of the rod in-bore. All these factors can drastically reduce penetration performance. While traditional weapon systems have sought to balance the advantages of higher impact L/D with the risks of higher launch L/D, an alternative is to employ NKEP technologies that change the L/D ratio in flight. These are launched with lower L/D but extend in-flight before impact, gaining the enhanced terminal effects of higher L/D.

There are many mechanisms to produce enhanced rod L/D through extension. One of the simplest mechanisms is to employ a split-sector type configuration, where the cross section of a cylindrical rod is split into mating sectors that slide laterally to achieve enhanced length. The terminal ballistic performance of many variants of split-sector configurations has been investigated (for example, see Hodge et al., 2004). The most basic configuration of the split-sector type is the rod-tube extender. However, the cavity produced by the fore section of the projectile will not necessarily allow the aft section to pass unimpeded (in fact this common to *all* extenders of the split-sector type). This is a severely limiting factor at ordinance velocity (up to 1.7 km/s). Hypervelocity enables extenders to perform much better because the larger cavity diameters permit the unimpeded passage of the aft section of the penetrator. In this paper, we demonstrate that this can be achieved for simple rod-tube extenders.

2. SETUP

Tungsten heavy alloy (WHA) was used as the penetrator material for all calculations and experiments in this paper. It was 91% tungsten, 7% nickel, 2% cobalt, and its properties have been previously reported (see, for example, Tarcza et al., 2004).

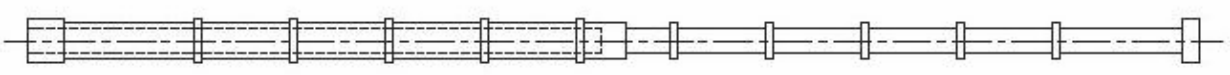

Figure 1. Rod-tube penetrator geometry

Report Documentation Page

Form Approved
OMB No. 0704-0188

1. REPORT DATE	2. REPORT TYPE	3. DATES COVERED
00 DEC 2004	**N/A**	**-**

4. TITLE AND SUBTITLE	5a. CONTRACT NUMBER
Novel Kinetic Energy Penetrators For Electromagnetic Guns	5b. GRANT NUMBER
	5c. PROGRAM ELEMENT NUMBER
6. AUTHOR(S)	5d. PROJECT NUMBER
	5e. TASK NUMBER
	5f. WORK UNIT NUMBER
7. PERFORMING ORGANIZATION NAME(S) AND ADDRESS(ES) **The Institute for Advanced Technology Austin, TX 78759**	8. PERFORMING ORGANIZATION REPORT NUMBER
9. SPONSORING/MONITORING AGENCY NAME(S) AND ADDRESS(ES)	10. SPONSOR/MONITOR'S ACRONYM(S)
	11. SPONSOR/MONITOR'S REPORT NUMBER(S)

12. DISTRIBUTION/AVAILABILITY STATEMENT
Approved for public release, distribution unlimited

13. SUPPLEMENTARY NOTES
See also ADM001736, Proceedings for the Army Science Conference (24th) Held on 29 November - 2 December 2005 in Orlando, Florida. , The original document contains color images.

14. ABSTRACT

15. SUBJECT TERMS

16. SECURITY CLASSIFICATION OF:			17. LIMITATION OF ABSTRACT	18. NUMBER OF PAGES	19a. NAME OF RESPONSIBLE PERSON
a. REPORT **unclassified**	b. ABSTRACT **unclassified**	c. THIS PAGE **unclassified**	**UU**	**7**	

An example of rod-tube extender geometry is shown in Fig. 1. This figure depicts a pre-extended shape designed for impact experiments. There are ten lands—raised sections along the body of the penetrator—that are used to mate with an aluminum sabot for launch from a two-stage light-gas gun at the IAT hypervelocity launch facility. The penetrator shown is machined from a single piece of WHA.

When considering geometry variants of any extender, critical dimensions to consider include not only L and D but also the collapsed length L_c. While collapsed length is not as critical to terminal ballistic performance as the extended length L, it is important to consider, since it controls the stresses during launch and the mass of the sabot. Furthermore, for rod-tube extenders the tube inner diameter D_I (equal to the rod outer diameter) must also be defined. Thus, two important dimensionless parameters controlling the geometry of rod-tube extenders are the extension ratio η, defined as L/L_c, and the diameter ratio μ, defined as D/D_I. Smaller diameter ratios partition a larger portion of mass to the tube and vice versa, with equal mass partitioning achieved for $\mu = \frac{\sqrt{2}}{2} \approx .7$.

Dimensions selected for the penetrators investigated in this study were an extended length L of 249 mm, a collapsed length L_c of 131 mm, and diameter D of 7.5 mm. Thus, the aspect ratio of the collapsed rod L_c/D is 17.5 and the extension ratio η is 1.9, allowing 10% of the collapsed length for extension and interlocking mechanisms (these will not be discussed in this paper). Diameter ratios in the range $0.6 \leq \mu \leq 0.9$ were considered to investigate the effect of mass partitioning on performance.

Two important metrics of the performance of rod-tube extenders also arise from the geometry definitions given above. The collapsed rod with a length L_c and diameter D is the unextended version of extended rod; the penetration of this rod is believed to represent a lower bound on the performance of the extended rod. Likewise, the baseline rod with the same mass and length of the extended rod is believed to represent an upper bound on the penetration performance of the extender. The diameter D_E of the baseline rod is the mass-equivalent diameter of the baseline rod defined as

$$D_E = \left(\frac{4M}{\pi \rho L} \right)^{1/2}, \qquad (1)$$

where ρ is the mass density. Since the two comparison rods and the extending rod are all equal in kinetic energy, the performance comparisons are on a per-unit-energy basis.

Another parameter strongly influencing terminal ballistic performance is the impact angle of attack α. After launch, the angle of attack tends to cycle through a slowly dampening oscillation, with α at impact being its value at some point in this cycle. Extending rods provide a means for rapid damping of this oscillation if extension is performed at the proper point in the cycle. While this advantage will help mitigate the terminal angle of attack, it will not completely eliminate it. Thus, it is important to consider how variations in α affect the performance.

While real-heavy armor targets contain complex geometries with multiple materials, it is important to demonstrate the utility of projectiles in penetrating simple monolithic targets. Only after enhanced performance against monolithic targets is demonstrated is it reasonable to consider more realistic armor configurations. As such, in this study only semi-infinite rolled homogeneous armor (RHA) targets are considered in the analysis.

Calculations described in this research were performed using the Eulerian finite volume hydrocode CTH, developed by Sandia National Laboratories. In previous work we have validated the accuracy of this code in predicting the penetration depth of a wide variety of WHA rod geometries (including extenders) penetrating RHA targets over a large velocity range. Fine zoning was maintained to insure numerically resolved computations; 0.375 mm zones were used for strong interaction regions in the penetrator and target, corresponding to approximately 20 zones across the diameter of the penetrator. Outside this region, zones were permitted to increase in size by a ratio of 1.05. The 3D calculations were performed primarily on a Compaq SC40/45 system (EV 6.8 processors) at the Aeronautical Systems Center Major Shared Resource Center at Wright-Patterson Air Force Base, OH. In total, 27 calculations were performed. Typical single runs used 64 processors and consumed between 640-3200 CPU hours each, depending on symmetry conditions (CPU time on a parallel computer system is defined as the runtime multiplied by the number of processors used). Some preliminary calculations were performed on an IBM SP-Power3 at the US Army Research Laboratory Major Shared Resource Center located at Aberdeen Proving Ground, MD using 64 processors where 5800 CPU hours were required for the smallest problems due to the slower processor speed.

3. EFFECT OF DIAMETER RATIO

Several quarter-symmetry calculations were first performed to determine the effect of diameter ratio on penetration. Diameter ratios ranging from $\mu = 0.6$ to $\mu = 0.9$ in $\mu = 0.1$ increments were considered. Effect of orientation was also considered; each of these calculations was performed with the tube section of the extender both fore and aft.

Results of these calculations are summarized in Fig. 2, where residual length of the rod is shown as a function of penetration depth. As penetration advances, the length of the penetrator is eroded starting from the impacting face and progressing to the tail of the penetrator, which is shown in Fig. 2. For comparison, the residual length history of the baseline rod is also shown. For the collapsed rod, only the final penetration depth is indicated on the graph (169 mm - with an initial length of 131 mm). Presenting the results in this way is very revealing since the slope of this line at any point is the inverse of the instantaneous penetration efficiency of the rod. It also clearly delineates contributions to penetration depth of the fore and aft sections of the penetrator, since a horizontal line intersecting the midpoint of the *y*-axis approximately separates the two sections. When the rod section impacts fore, for example, the penetration efficiency is nearly equal to that obtained for the baseline rod. Only during the late stages of penetration, when the tube section begins to penetrate, is the penetration efficiency reduced. Large diameter ratios result in very poor performance of the tube section. On the other hand, when the rod section is shot aft, the penetration efficiency of the tube section is significantly lower than the value for the baseline rod, and decreases as the diameter ratio increases. For $\mu \leq 0.8$, the reduction is significant. Improved penetration efficiency, comparable to the baseline rod, is achieved by the rod section during late stages of penetration, but surprisingly there is significant efficiency reduction during the early phase of rod section penetration.

It is important to note that extension enhances the penetration performance of the rod-tube in all cases. The performance enhancement ranges from as little as 7% for the tube-first μ =0.9 case to 70% for the rod-first μ =0.6 case. This corresponds to a P/L_c ranging from 1.38 to 2.20.

All the tube-first simulations (indicated by unfilled shapes) show immediate degradation of performance compared to baseline case in penetration. The thicker-walled tubes ($\mu \leq 0.7$) show less immediate degradation, but then a sudden drop off in performance when the smaller-diameter rod begins penetration. The thinner-walled tubes ($\mu \geq 0.8$) show very poor initial penetration but then much better penetration after the rod portion has cleared the debris from the tube and is only being eroded by penetrating the RHA. The μ = 0.6 and μ = 0.7 cases have nearly identical total penetration, both of which are better than the μ = 0.8 and μ = 0.9 cases, which are also nearly identical.

All the rod-first simulations (indicated by filled shapes) show near-ideal penetration until the tube section begins penetration (at about 125 mm residual length). From this point on, there is a gradual drop in performance that only becomes significant in the last half of the tube section.

Material plots are helpful in understanding the behavior leading to the differences in penetration efficiency seen in Fig. 2. A series of material plots for μ = .7 is shown in Figs. 3–6. In Fig. 3, a plot of materials 120 μs after impact with the rod section fore is shown. At this stage of penetration, the rod section is nearly completely eroded. In Fig. 4, a material plot is shown at

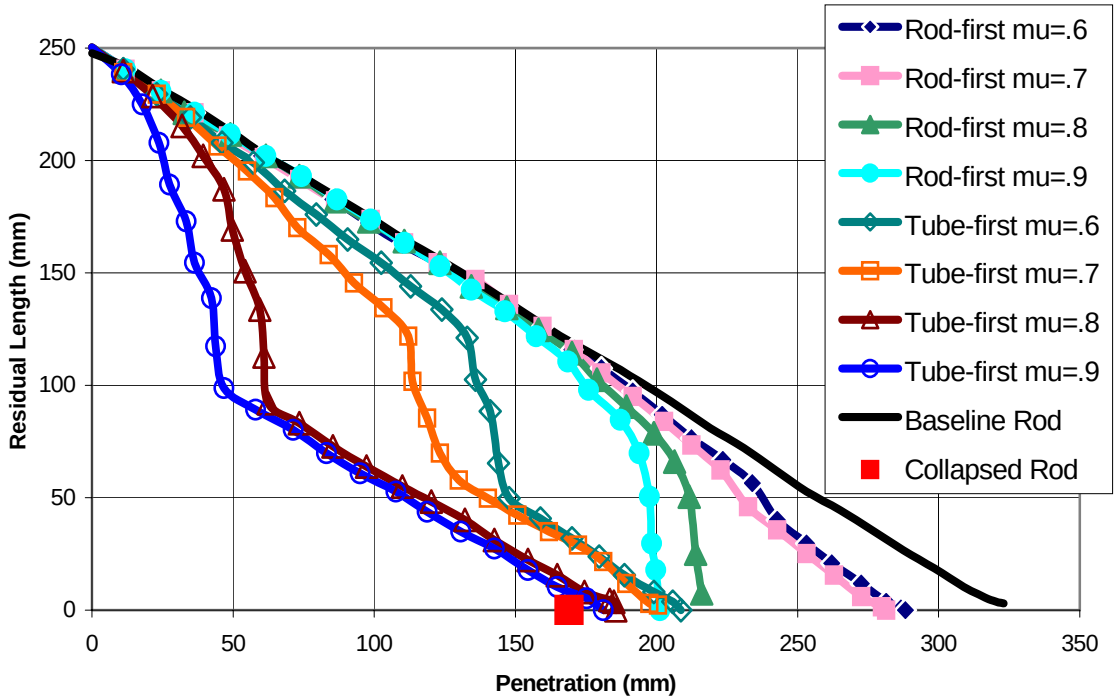

Figure 2. Penetration vs. residual length for rod-tubes.

the same time with the tube section fore. As is evident, the cavity produced by the tube section is not as deep as that produced by the rod (this efficiency reduction was also evident in Fig. 2). Evidently, at this diameter ratio the tube wall thickness is not sufficient to choke the flow of target debris. As a result, the trailing rod must first penetrate this debris before reaching the base of the crater. This leads to the significant reduction in efficiency seen during the early stages of rod penetration when the tube is shot fore.

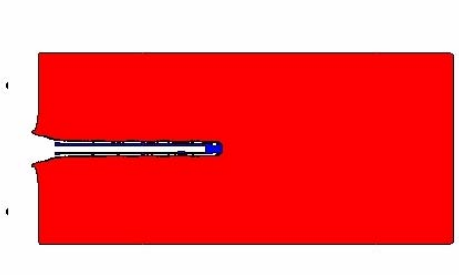

Figure 3. Rod first, $\mu = 0.7$, time = 120 μs.

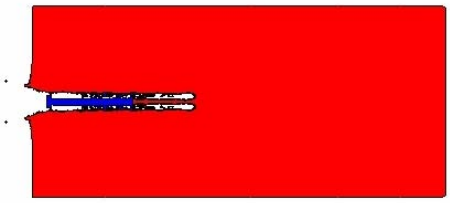

Figure 4. Tube first, $\mu = 0.7$, time = 120 μs.

Fig. 5 shows the same simulation as Fig. 3, only at late time. The penetration of the tube section is similar to that in Fig. 4, except that the flow of debris up the center of the tube does not cause the problems that it did for the tube-first penetrator. Fig. 6 shows the same simulation as Fig. 4, but at late time. Clearly, the debris formed by the tube section has interfered with the penetration of the rod section. The spurs formed along the crater walls are evidence of inefficient penetration.

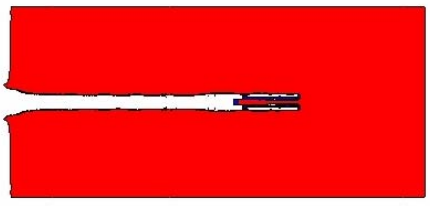

Figure 5. Rod first, $\mu = 0.7$, time = 200 μs.

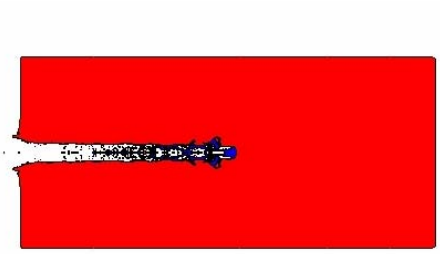

Figure 6. Tube first, $\mu = 0.7$, time = 200 μs.

In the $\mu = 0.7$ simulations shown in Figs. 3–6, the tube penetration is not quite steady state, as evidenced by the small sidewall craters. These craters are one cause of the penetration efficiency reduction for tubes seen in Fig. 2. Thinner-walled tubes exhibit more severe efficiency reductions compared to the moderate reductions seen for thicker walls. The efficiency reduction is apparently the result of unstable penetration by the tube for $\mu \leq 0.8$. Shown in Fig. 7 is a material plot 80 μs after impact with the tube section fore and $\mu = 0.8$. As is evident, the cavity diameter opened by the tube diverges and the penetration progresses, leading to the sharp reduction in efficiency seen in Fig. 2.

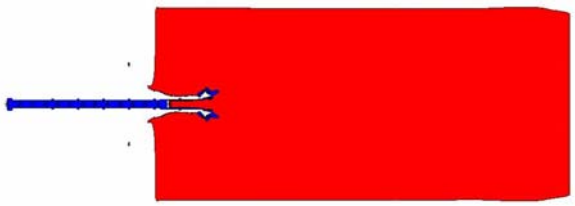

Figure 7. Tube first, $\mu = 0.8$, time = 80 μs.

The thinner-walled tubes ($\mu \geq 0.8$) show much greater degradation in performance than those with thicker walls. The thicker-walled rods, $\mu = 0.6$ and $\mu = 0.7$, complete with 288 mm and 281 mm of total penetration respectively.

From this set of calculations, it is apparent that rod-first is the best direction to fire the penetrator. All rod-first calculations performed better than the corresponding tube-first calculation.

At this point in this study it was necessary to choose a μ for further analysis. Since the total performance difference between $\mu = 0.6$ and $\mu = 0.7$ was negligible, there was not sufficient justification for varying the geometry from the default equal mass distribution of $\mu = \frac{\sqrt{2}}{2}$.

4. AOA ANALYSIS

A set of CTH calculations was performed to analyze the AoA sensitivity of the rod-tubes. To validate the previous conclusion that rod-first was the optimal direction to fire the projectile, both rod-first and tube-first directions were again examined. Simulations were run with half symmetry; yaw varied from 0°–2° in 0.5° increments. The results are shown in Fig. 8.

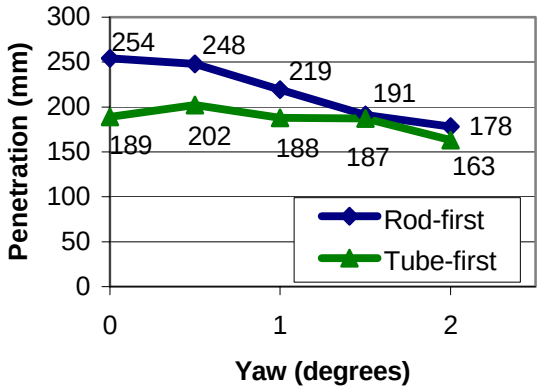

Figure 8. Penetration vs. AoA from CTH.

As can be seen in Fig. 8, rod-first again is the optimal direction of impact. All rod-first tests performed better than the corresponding tube-first test. However, it is interesting to notice the low AoA sensitivity of the tube-first tests. This is understandable, since the wider crater opened by the tube should allow the thinner rod to pass through unimpeded, even with higher AoA.

The rod-first simulations showed much greater sensitivity to AoA, especially at 1° and beyond. This is because the smaller crater created by the rod does not have as much tolerance for the larger-diameter tube to pass through unimpeded. Though the sensitivity to AoA was higher with the rod-first launch, the overall performance was still better than tube-first.

5. EXPERIMENTAL RESULTS

In order to verify the CTH predictions, two laboratory experiments were conducted at the IAT hypervelocity launch facility. In both experiments, the equal-mass-distribution version of the rod/tube was launched at semi-infinite RHA. Unfortunately, neither experiment quite achieved the desired velocity of 2.2 km/s. Shot 790 impacted at 2.14 km/s with 0.8° AoA and penetrated 208 mm. Shot 797 impacted at 2.16 km/s with 0.6° AoA and penetrated 199 mm. These values are plotted in Fig. 9.

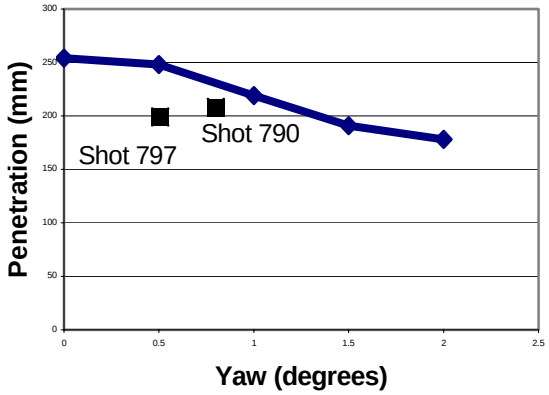

Figure 9. Penetration vs. AoA showing experimental data.

The experimental data is clearly not as favorable for penetration as the CTH data. One factor contributing to this degraded performance is probably the lower impact velocity. The targets are shown in Figs. 10 and 11, with the CTH craters for 0.5° and 1.0° AoA shown in Figs. 12 and 13 for comparison. The differences are chiefly in the lower part of the channel made by the tube. While the simulations show limited gouging of the tube crater, the experimental craters are very rough. This is presumably due to fracture of the penetrator, which is not accurately modeled by the code. Perhaps the use of a more ductile alloy would have resulted in a more uniform channel (as in the simulations) and greater total penetration.

Figure 10. Shot 790 crater cross section.

Figure 11. Shot 797 crater cross section.

Figure 12. CTH, 0.5° AoA crater cross section.

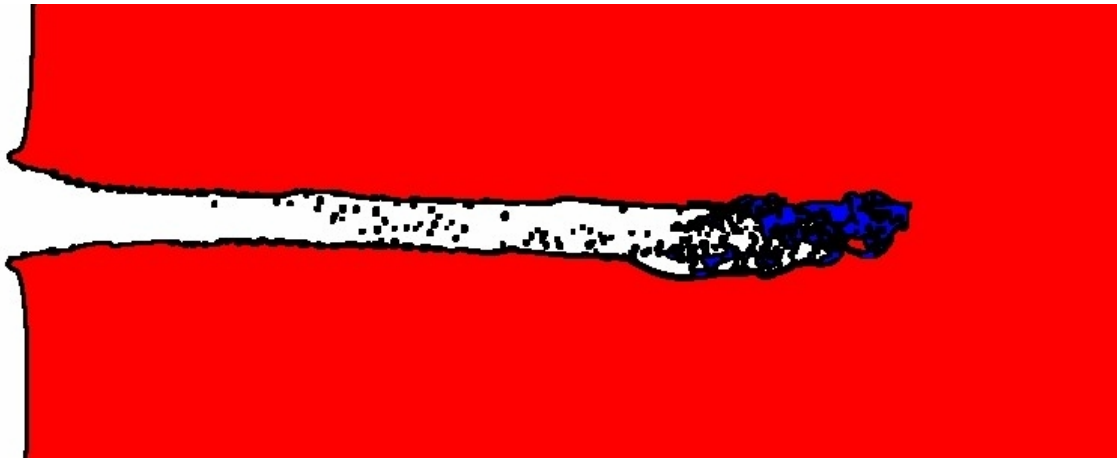

Figure 13. CTH, 1.0° AoA crater cross section.

6. CONCLUSION

This paper has described the performance of a rod-tube extending penetrator. This was done not to suggest actual implementation of rod-tubes as a projectile, but as a guide to the behavior of a broader class of extending projectiles for FCS application. It was shown that with proper design, the penetration of a rod-tube can exceed that of a collapsed rod by as much as 70%. For fixed penetration, this can allow for a much lower-mass projectile, which is the primary motivation for pursuing extenders for EM guns. Since the maximum feasibly launchable *L/D* is relatively fixed, a 70% increase in performance corresponds to a penetrator with approximately 1/5 the mass of a standard rod (since both *L* and *D* must increase by 70% to match the performance of the extender). While an analysis of parasitic mass (mass launched besides the projectile, such as the armature and sabot) is beyond the scope of this paper, a reasonable first-order approximation of parasitics is that they are equal in mass to the penetrator (Zielinski and Parker, 1999). This assumption indicates that the launch package for the rod-tube will have also have a mass of 1/5 of the launch package mass for a larger rod capable of the same penetration. This thereby cuts the launch energy by 4/5. While EM launch system design is again out of the scope of this paper, a first-order approximation of scaling is that the mass and volume of power supply, cooling, and other dependent systems scale linearly with launch energy. It is this savings of energy in the EM launch system size and mass that makes extending penetrators very appealing for use in EM guns. Cutting the EM launch system size by 80% makes EM guns a candidate for implementation in future FCS upgrades.

REFERENCES

Hodge, J. L., Littlefield, D. L., and Subramanian, R. “The Effect of Impact Velocity on the Performance of Extending Penetrators,” presented at the 15th US Army Ground Vehicle Survivability Symposium (GVSS), March 29-April 1, 2004, Monterey, California. IAT.P 0688.

Tarcza, K., Bless, S., and Taleff, E. “Fracture of Tungsten Rods,” presented at this conference. IAT.P 0725.

Zielinski, A.E., Parker, J.V.; “Penetrator Coupling for a Mass Efficient Integrated Launch Package,” Institute for Advanced Technology, The University of Texas at Austin. IAT.R 0198, September 1999.